Geomechanics and Engineering, *Vol. 29, No. 6 (2022) 667-681*
https://doi.org/10.12989/gae.2022.29.6.667

Thermoelastic analysis of rectangular plates with variable thickness made of FGM based on TSDT using DQ method

Majid Amiri[a], Abbas Loghman[b] and Mohammad Arefi*

Department of Solid Mechanic, Faculty of Mechanical Engineering, University of Kashan, Kashan 87317-51167, Iran

(Received November 2, 2021, Revised April 13, 2022, Accepted May 2, 2022)

Abstract. This paper presents a thermoelastic analysis of variable thickness plates made of functionally graded materials (FGM) subjected to mechanical and thermal loads. The thermal load is applied to the plate as a temperature difference between the top and bottom surfaces. Temperature distribution in the plate is obtained using the steady-state heat equation. Except for Poisson's ratio, all mechanical properties of the plate are assumed to vary linearly along the thickness direction based on the volume fractions of ceramic and metal. The plate is resting on an elastic foundation modeled based on the Winkler foundation model. The governing equations are derived based on the third-order shear deformation theory (TSDT) and are solved numerically for various boundary conditions using the differential quadrature method (DQM). The effects of various parameters on the stress distribution and deflection of the plate are investigated such as the value of thermal and mechanical loads, volume fractions of ceramic and metal, and the stiffness coefficients of the foundation.

Keywords: differential quadrature method; functionally graded material; thermoelastic analysis; third-order shear deformation theory

1. Introduction

FGMs are new composites made of two or more phases in which their mechanical properties vary smoothly and continuously in a particular direction (Huo *et al.* 2021, Moradi *et al.* 2021, Shao *et al.* 2021). A FGM composite is a combination of ceramic and metal. The mechanical properties, such as modulus of elasticity, density, thermal conductivity coefficient, etc., are presented in terms of volume fractions of constituent and local coordinate of structure made of them (Dai *et al.* 2021, Habibi *et al.* 2021, Zhang *et al.* 2021a). In laminated composites, material properties vary discontinuously across adjoining layers. Therefore, thermal stress concentration in these areas causes joint layer surface problems. These problems can be removed by continuously changing the properties of the materials, which is a characteristic of FGMs (Bai *et al.* 2020, Dai *et al.* 2021, Najaafi *et al.* 2021).

The plates made of FGMs have unique properties, such as high-temperature resistance, corrosion resistance, wear and fracture resistance and are used in aerospace, power plant, and petrochemical industries (Liu *et al.* 2020, Wang *et al.* 2020). A literature review is presented in this section to show the importance of this study. Reddy *et al.* (1999) investigated relations between the bending solutions of the FGM circular plates modeled based on the classical plate theory (CPT) and the first-order shear deformation theory (FSDT). Ma and Wang (2004) compared the TSDT and CPT to analyze the bending and buckling of FGM circular plates in order to examine which theory is enough to consider the effect of shear deformation on the axisymmetric bending and bucking of FGM circular plates. Nie and Zhong (2007) analyzed the dynamic responses of an FGM circular plate with various boundary conditions based on the three-dimensional theory of elasticity. Three-dimensional analysis of a FGM plate was investigated by Zhong and Shang (2008). They assumed that the modulus of elasticity varies in the thickness direction. Li *et al.* (2008) studied the bending analysis for a transversely isotropic FGM circular plate subjected to an axisymmetric transverse load. An exact relation between the deflection of the plate and different FG plate theories was examined by Cheng and Batra (2000). They investigated deflections of a simply supported FG polygonal plate. Lu *et al.* (2009) presented semi-analytical three-dimensional elasticity solutions for orthotropic multi-directional FG plates. For the solution method, they used the DQM based on state-space formalism. Beena and Parvathy (2014) investigated the development of the spline finite strip method for analyzing FGM plates.

Carrera (2002) presented an overview of 3-D approaches, 2-D theories and finite elements that have been allocated for multilayered, anisotropic, composite plate and shell structures. Most of his study was assigned to axiomatic theories and related finite element performances. Deformations of a simply supported FG plate were investigated by Brischetto *et al.* (2008), in which thermo-mechanical loadings were applied to the plate. Ching and Yen (2005) analysed the meshless local Petrov-Galerkin

*Corresponding author, Associate Professor
E-mail: arefi63@gmail.com; arefi@kashanu.ac.ir
[a]Ph.D. Student
[b]Professor

ISSN: 2005-307X (Print), 2092-6219 (Online)

(MLPG) approach for 2D functionally graded solids. They employed the penalty method to execute the necessary boundary conditions. Zenkour (2009) utilized refined sinusoidal deformation theory to analyze the thermal bending of an FG plate, which was subjected to a transverse uniform load and a temperature field. It was resting on the Pasternak foundation. Zenkour (2018) presented hygro-thermo-mechanical bending analysis of a variable thickness thin plate. He used Levy's approach and the small parameter method to solve the problem. Tounsi *et al.* (2020) studied the static behavior of an advanced functionally graded (AFG) ceramic-metal plate. The plate was subjected to a nonlinear hygro-thermo-mechanical load resting on the Winkler-Pasternak foundation. They discussed the effects of temperature, moisture concentration, and volume fraction variation on the mechanical behavior of AFG plates. Refrafi *et al.* (2020) focused on an FG sandwich plate's mechanical and hygrothermal buckling analysis resting on a two-parameter elastic foundation. They investigated the effects of the temperature, moisture concentration, and the inhomogeneity parameter on the critical buckling of such structures. Matouk *et al.* (2020) studied the vibration characteristics of the FG nano-beams located in the hygro-thermal environment and resting on the elastic foundation. They provided a parametric study to examine the effects of the various parameters on the natural frequencies, such as power-law index and hygro-thermal loading. There are some applications of new materials and structures in new engineering applications based on the various references (Mou *et al.* 2018, Ali *et al.* 2022, Yu *et al.* 2021, Zhang *et al.* 2015, 2017, 2018, 2021b, c, 2022, Wei *et al.* 2021, Xiao *et al.* 2022a, Wang *et al.* 2022a, Huang *et al.* 2022, Li *et al.* 2017, Shiping *et al.* 2021, Yang *et al.* 2017, 2019a, b, Jia *et al.* 2014, Chen *et al.* 2021, Casmed *et al.* 2021, Liu *et al.* 2021b, Lu *et al.* 2021, Xiao *et al.* 2022b, Qiao *et al.* 2021, 2022).

Bellifa *et al.* (2021) studied the effect of porosity on the nonlinear thermal stability response FG beam with different boundary conditions. Merazka *et al.* (2021) focused on the hygro-thermo-mechanical bending analysis of the FG plate seated on the Winkler-Pasternak foundation. The influences of the moisture concentration, temperature, and power-law index on the deflection and shear stresses were discussed. Tounsi *et al.* (2021) presented an exact solution for hygro-thermo-mechanical bending characteristics of perfect and imperfect AFG ceramic-metal plates. They studied the influences of hygro-thermal loading and imperfection on the deflection of the plate. The free vibrational analysis of an FG sandwich plate resting on a viscoelastic foundation and subjected to a hygrothermal environment was studied by Zaitoun *et al.* (2021). They concluded that the increase in the viscoelastic foundation's damping coefficient develops the plate's free-vibrational response. Some solution methods of applicable problems and some mathematical methods for solution of the governing equations can be observed in literature (Nazeer *et al.* 2021, Chu *et al.* 2021, Zhao *et al.* 2021b, c, Iqbal *et al.* 2022, Wang *et al.* 2020, 2022b, Chu *et al.* 2021, Rashid *et al.* 2022a, b, Song *et al.* 2015, Hajiseyedazizi *et al.* 2021. Jin *et al.* 2022). Mudhaffar *et al.* (2021) studied the static bending analysis of an AFG ceramic–metal plate subjected to a hygro-thermo-mechanical load and resting on a three-parameter viscoelastic foundation. They discussed the influences of the power-law index, moisture concentration and temperature on the AFG plate's bending response. Wave propagation characteristics of a porous FG ceramic-metal sandwich plate with different distributions in porosity and subjected to a hygro-thermal environment were examined by Tahir *et al.* (2021). Zaitoun *et al.* (2022) studied the buckling analysis of an FG sandwich plate resting on a two-Pasternak foundation coefficient model and exposed to hygrothermal loading. They investigated the effects of the damping coefficient, moisture condition, power-law index, and temperature variation on the buckling characteristics of such a structure.

In recent years, many studies have been done on the analysis of FGM plates using new numerical methods such as the DQM. Still, investigations show that thermoelastic analysis of variable thickness FGM plates resting on the elastic foundation utilizing DQM has not been presented. This study aims to investigate the effective parameters in the thermoelastic analysis of variable thickness plates and the DQM is used to solve the governing equations.

1. 2. Loading, geometry, and material properties

The hypotheses used in this study are:

1. The plate is thin, and the thickness of the plate is variable in spatial x direction.

2. The material's behavior is assumed to be linearly elastic and follows Hooke's law. By considering the assumption of linearity, the plate's response to the combination of thermal and mechanical loads can be acquired using the superposition method.

3. The heat load is applied as a temperature difference between the top and bottom of the plate.

4. The foundation is simulated based on the Winkler foundation model.

5. The mechanical and thermal properties of the material are functionally graded in the thickness direction employing the volume fraction ratio.

6. The mechanical and thermal properties of the plate are temperature independent.

The plate is subjected to thermal and mechanical loads. The mechanical and thermal properties vary along the thickness direction continuously. The mechanical load is distributed sinusoidally. The temperature varies increasingly and nonlinearly along the thickness direction and each point's temperature is considered to be constant. The distribution of silicon carbide particles C(z) is supposed to vary along the thickness direction using a linear scheme (Golmakaniyoon and Akhlaghi 2016)

$$C(z) = C_{\min} + \left(C_{\max} - C_{\min}\right)V_c$$
$$V_c = \frac{z}{h} + \frac{1}{2} \tag{1}$$

in which C_{max} and C_{min} are silicon carbide's volume fractions at the top and bottom of the plate, respectively.

Based on the defined volume fraction in Eq. (1), the variable material properties such as modulus of elasticity and thermal conductivity coefficient are described along the thickness direction as follows

$$P(z) = P_{Al} + (P_{SiC} - P_{Al})C(z) \tag{2}$$

P (z) is assumed to be a material property of the FGM plate (except the Poisson's ratio) (Chung and Chen 2007). P_{Al} and P_{sic} are the specified properties of pure aluminum and pure silicon carbide, respectively. Poisson's ratio is considered to be constant because the influence of Poisson's ratio on the deformation of FGM plates is much less than that of the modulus of elasticity. Variable modulus of elasticity is as follows (Barati 2017, Kiani, Gharebaghi *et al.* 2017, Sobhy 2017, Hosseini-Hashemi and Khaniki 2018, Ahmadi and Foroutan 2019)

$$E(z) = E_{Al} + (E_{SiC} - E_{Al})C(z) = E_{Al} + (E_{SiC} - E_{Al}) \left[C_{\min} + (C_{\max} - C_{\min}) \left(\frac{z}{h} + \frac{1}{2} \right) \right] \tag{3}$$

The length and width of the plate are a and b, respectively, and the thickness is variable along the x-axis h=h(x) and the plate is rested on the Winkler elastic foundation.

Variation of plate's thickness is expressed by a particular function as follows

$$h(x) = h_0 \left(1 - \beta \frac{x}{a} \right) \tag{4}$$

The mechanical and thermal load properties are assumed as follows

$$\begin{aligned} &a = 1m, \quad \frac{b}{a} = 1, \quad h(x) = h_0 \left(1 - \beta \frac{x}{a} \right), \quad \frac{h_0}{a} = 0.02, \quad \beta = 0.1, \\ &E_m = 70GPa, \quad K_m = 237 \frac{W}{mC}, \quad \alpha_m = 23.1 \times 10^{-6} \frac{1}{K}, \\ &E_c = 410GPa, \quad K_c = 120 \frac{W}{mC}, \quad \alpha_c = 4 \times 10^{-6} \frac{1}{K}, \\ &v = 0.25, \quad k_w = 50 \frac{MN}{m^3}, \\ &C_{\min} = 0.2, \quad C_{\max} = 0.35, \\ &T_0 = 300K, \quad T_{bottom} = 310K, \quad T_{top} = 320K. \end{aligned} \tag{5}$$

3. Temperature loading

The steady-state one-dimensional heat equation without heat flux is given by

$$-\frac{d}{dz} \left[K(z) \frac{dT}{dz} \right] = 0 \tag{6}$$

The differential equations are solved with the following assumptions

$$\begin{aligned} K(z) &= K_{Al} + (K_{SiC} - K_{Al})C(z) \\ C(z) &= C_{\min} + (C_{\max} - C_{\min})V_c \end{aligned} \tag{7}$$

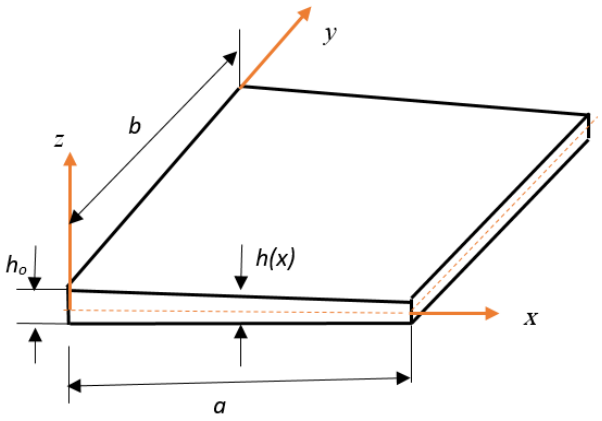

Fig. 1 The geometry of a plate with thickness varies along the x-axis direction

The required boundary conditions are considered to be as

$$\begin{aligned} T\left(\frac{h}{2} \right) &= T_c \\ T\left(-\frac{h}{2} \right) &= T_m \end{aligned} \tag{8}$$

By solving the heat equation and applying the boundary conditions, the temperature distribution is obtained as

$$\begin{aligned} T(z) &= \frac{c_1 h}{\beta_2} Ln \left[1 + \frac{\beta_2}{\beta_1} \left(\frac{z}{h} + \frac{1}{2} \right) \right] + c_2 \\ \beta_1 &= K_m + K_{cm} C_{\min} \\ \beta_2 &= K_{cm} C_{cm} \\ T\left(-\frac{h}{2} \right) &= T_{bottom} \rightarrow c_2 = T_{bottom} \\ T\left(\frac{h}{2} \right) &= T_{top} \rightarrow c_1 = \frac{\beta_2 (T_{top} - T_{bottom})}{hLn \left(1 + \frac{\beta_2}{\beta_1} \right)} \end{aligned} \tag{9}$$

Nonlinearity variation for temperature distribution along the thickness direction is shown in Eq. (9).

4. Governing equations and boundary conditions

The displacement field based on the TSDT is assumed as follows

$$\begin{aligned} u(x,y,z) &= z\varphi(x,y) - c_1 z^3 \left[\varphi(x,y) + w_x(x,y) \right] \\ v(x,y,z) &= z\psi(x,y) - c_1 z^3 \left[\psi(x,y) + w_y(x,y) \right] \\ w(x,y,z) &= w_0(x,y) \\ c_1 &= \frac{4}{3h^2(x)} \end{aligned} \tag{10}$$

As shown in Eq. (10), the thickness-stretching is neglected $(\varepsilon_{zz} = 0)$ (Reddy 2007).

The strain-displacement relations are as follows

$$\begin{aligned}\varepsilon &= \left\{\varepsilon_x \quad \varepsilon_y \quad \gamma_{xy}\right\}^T = \varepsilon^{(0)} + z\,\varepsilon^{(1)} + z^3\varepsilon^{(3)} - \varepsilon^{(t)},\\ \gamma &= \left\{\gamma_{yz} \quad \gamma_{xz}\right\}^T = \gamma^{(0)} + z^2\gamma^{(2)},\end{aligned} \tag{11}$$

in which

$$\begin{aligned}\varepsilon^{(0)} &= \begin{Bmatrix}0\\0\\0\end{Bmatrix}, \varepsilon^{(1)} = \begin{Bmatrix}\varphi_x\\ \psi_y\\ \varphi_y + \psi_x\end{Bmatrix}, \varepsilon^{t} = \begin{Bmatrix}\alpha\Delta T\\ \alpha\Delta T\\ 0\end{Bmatrix},\\ \varepsilon^{(3)} &= -\begin{Bmatrix} c_{1x}\left(\varphi + w_x\right) + c_1\left(\varphi_x + w_{xx}\right)\\ c_1\left(\psi_y + w_{yy}\right)\\ c_{1x}\left(\psi + w_y\right) + c_1\left(\varphi_y + \psi_x + 2w_{xy}\right)\end{Bmatrix}\end{aligned} \tag{12}$$

and

$$\gamma^{(0)} = \begin{Bmatrix}\gamma^0_{yz}\\ \gamma^0_{xz}\end{Bmatrix} = \begin{Bmatrix}\psi + w_y\\ \varphi + w_x\end{Bmatrix}, \quad \gamma^{(2)} = -3c_1\begin{Bmatrix}\psi + w_y\\ \varphi + w_x\end{Bmatrix}, \tag{13}$$

Stress-strain relations are as below (Arefi and Rahimi 2011,2012,2014, Arefi *et al*. 2011, 2018, Khoshgoftart *et al*. 2013, Arefi and Nahas 2014 Arefi 2014, Heidari *et al*. 2021 Kholdi *et al*. 2022)

$$\begin{aligned}&\sigma = D_m(z)\left(\varepsilon^{(0)} + z\,\varepsilon^{(1)} + z^3\varepsilon^{(3)} - \varepsilon^{(t)}\right),\\ &\sigma = \left\{\sigma_x \quad \sigma_y \quad \tau_{xy}\right\}^T\\ &\tau = D_s(z)\left(\gamma^{(0)} + z^2\gamma^{(2)}\right), \quad \tau = \left\{\tau_{yz} \quad \tau_{xz}\right\}^T,\\ &D_m(z) = \frac{E(z)}{1-\upsilon^2}\begin{bmatrix}1 & \upsilon & 0\\ \upsilon & 1 & 0\\ 0 & 0 & \dfrac{1-\upsilon}{2}\end{bmatrix},\\ &D_s(z) = \frac{E(z)}{2(1+\upsilon)}\begin{bmatrix}1 & 0\\ 0 & 1\end{bmatrix}.,\end{aligned} \tag{14}$$

Based on the stress relations, the resultant components are derived as (Moradi *et al*. 2021)

$$\begin{aligned}\begin{Bmatrix}\tilde{M}\\ \tilde{P}\\ \tilde{Q}\\ \tilde{R}\end{Bmatrix} &= \begin{bmatrix}B & D & F & 0 & 0\\ E & F & H & 0 & 0\\ 0 & 0 & 0 & \hat{A} & \hat{B}\\ 0 & 0 & 0 & \hat{B} & D\end{bmatrix}\begin{Bmatrix}\varepsilon^{(0)}\\ \varepsilon^{(1)}\\ \varepsilon^{(3)}\\ \gamma^{(0)}\\ \gamma^{(2)}\end{Bmatrix} -\\ &\begin{bmatrix}B & 0 & 0 & 0 & 0\\ E & 0 & 0 & 0 & 0\\ 0 & 0 & 0 & 0 & 0\\ 0 & 0 & 0 & 0 & 0\end{bmatrix}\begin{Bmatrix}\varepsilon^{t}\\ 0\\ 0\\ 0\\ 0\end{Bmatrix},\end{aligned} \tag{15}$$

in which

$$\tilde{M} = \begin{Bmatrix}M_x\\ M_y\\ M_{xy}\end{Bmatrix}, \quad \tilde{P} = \begin{Bmatrix}P_x\\ P_y\\ P_{xy}\end{Bmatrix}, \quad \tilde{Q} = \begin{Bmatrix}Q_y\\ Q_x\end{Bmatrix}, \quad \tilde{R} = \begin{Bmatrix}R_y\\ R_x\end{Bmatrix} \tag{16}$$

and

$$\begin{aligned}\left(A, B, D, E, F, H\right) &= \int_{-\frac{h(x)}{2}}^{\frac{h(x)}{2}}\left(1, z, z^2, z^3, z^4, z^6\right)D_m(z)\,dz\\ \left(\hat{A}, \hat{B}, D\right) &= \int_{-\frac{h(x)}{2}}^{\frac{h(x)}{2}}\left(1, z^2, z^4\right)D_s(z)\,dz\end{aligned} \tag{17}$$

Finally, the governing equations are derived as below (Reddy 2007)

$$\begin{aligned}&\frac{\partial Q_x}{\partial x} + \frac{\partial Q_y}{\partial y} - 3c_1\left(\frac{\partial R_x}{\partial x} + \frac{\partial R_y}{\partial y}\right) +\\ &c\left(\frac{\partial^2 P_x}{\partial x^2} + 2\frac{\partial^2 P_{xy}}{\partial x\,\partial y} + \frac{\partial^2 P_y}{\partial y^2}\right) + Q - kw = 0\\ &\frac{\partial M_x}{\partial x} + \frac{\partial M_{xy}}{\partial y} - c_1\left(\frac{\partial P_x}{\partial x} + \frac{\partial P_{xy}}{\partial y}\right) - Q_x + 3cR_x = 0\\ &\frac{\partial M_{xy}}{\partial x} + \frac{\partial M_y}{\partial y} - c_1\left(\frac{\partial P_{xy}}{\partial x} + \frac{\partial P_y}{\partial y}\right) - Q_y + 3cR_y = 0\end{aligned} \tag{18}$$

Substitution of Eqs. (11) and (17) into Eq. (18) results in the following relations

$$\begin{aligned}&Z_{11}w_x + Z_{12}w_{xx} + Z_{13}w_{xxx} + Z_{14}w_{xxxx} + Z_{15}w_{xyy} + Z_{16}w_{xxyy}\\ &+Z_{17}w_{yyyy} + Z_{18}w_{yy} - kw\\ &+Z_1\phi + Z_2\phi_x + Z_3\phi_{xx} + Z_4\phi_{xxx} + Z_5\phi_{xyy} + Z_6\phi_{yy} + Z_7\psi_y\\ &+Z_8\psi_{xy} + Z_9\psi_{xxy} + Z_{10}\psi_{yyy} = f_1\\ &S_7w_x + S_8w_{xx} + S_9w_{xxx} + S_{10}w_{xyy} + S_{11}w_{yy} + S_1\phi + S_2\phi_x\\ &+S_3\phi_{xx} + S_4\phi_{yy} + S_5\psi_y + S_6\psi_{xy} = f_2\\ &R_7w_y + R_8w_{xy} + R_9w_{xxy} + R_{10}w_{yyy} + R_1\phi_y + R_2\phi_{xy} + R_3\psi\\ &+R_4\psi_x + R_5\psi_{xx} + R_6\psi_{yy} = f_3\end{aligned} \tag{19}$$

in which f_1, f_2 and f_3 are as follows: G, and D~ in the above equations

$$\begin{aligned}f_1 &= \frac{c_1}{1-\nu}\left(\frac{\partial^2 M^{3T}}{\partial x^2} + \frac{\partial^2 M^{3T}}{\partial y^2}\right) - Q\\ f_2 &= \frac{1}{1-\nu}\frac{\partial M^T}{\partial x} - \frac{c_1}{1-\nu}\frac{\partial M^{3T}}{\partial x}\\ f_3 &= \frac{1}{1-\nu}\frac{\partial M^T}{\partial y} - \frac{c_1}{1-\nu}\frac{\partial M^{3T}}{\partial y}\end{aligned} \tag{20}$$

And the rest of the coefficients can be found in Appendix.

In this paper, different combination of simply supported and clamped boundary conditions for each edge of the plate are investigated. Therefore, simply supported boundary condition of the plate using TSDT is as

$$x = 0, a \rightarrow \begin{cases} \\ w = 0\\ \psi = 0\\ \left(\alpha_{12} - c\alpha_4\right)\phi_x - c\alpha_4 w_{xx} - c_x\alpha_4\left(\phi + w_x\right)\\ -\dfrac{M^T}{1-\nu} = 0\\ \alpha_6\phi_x + \alpha_7 w_{xx} + \alpha_8\left(\phi + w_x\right) - \dfrac{M^{3T}}{1-\nu} = 0\end{cases} \tag{21}$$

$$y=0,b\rightarrow\begin{cases}w=0\\ \phi=0\\ (\alpha_{12}-c\alpha_4)\psi_y-c\alpha_4 w_{yy}-\dfrac{M^T}{1-\nu}=0\\ \alpha_6\psi_y+\alpha_7 w_{yy}-\dfrac{M^{3T}}{1-\nu}=0\end{cases}$$

And for clamped boundary condition, is as follows

$$\begin{aligned}x=0,a\rightarrow&\begin{cases}w=0\\ \dfrac{\partial w}{\partial x}=0\end{cases}\\ y=0,b\rightarrow&\begin{cases}w=0\\ \dfrac{\partial w}{\partial y}=0\end{cases}\end{aligned}\qquad(22)$$

5. Solution procedure

The DQM was introduced by Bellman *et al.* (1972) in the 1970s and was employed by other authors to solve various problems in mechanical engineering (Al-Furjan *et al.* 2020a, b, Al-Furjan *et al.* 2020, Huang *et al.* 2021, Adab and Arefi 2022, Adab *et al.* 2022). This method is employed in this section to solve the governing equations in various boundary conditions. In comparison with the DQM, other numerical methods such as the finite element method (FEM), Rayleigh-Ritz method, or Galerkin method are stronger and more applicable in the mechanical analysis of problems with complicated geometrical shapes. But, these methods use the integral operator that provides high computational effort compared to the DQM. Consequently, for the problems with simple geometrical shapes (like a rectangular plate), it is more convenient to utilize the DQM (Nasution *et al.* 2022).

As shown in Eq. (23), the values of the two-dimensional function $F(x,y)$ can be presented as a set of the pre-selected grid of points (Liu *et al.* 2020, Shi *et al.* 2020)

$$F_{ij}=F(x_i,y_i),\quad i=1,2,...,N_x.\quad j=1,2,...,N_y.\qquad(23)$$

The derivative function can be estimated in function values at these points as (Torabi and Afshari 2017, Ghorbanpour Arani *et al.* 2019, Ghorbanpour Arani *et al.* 2021, Huang *et al.* 2021)

$$\left[\frac{\partial^{r+s}F}{\partial x^r\partial y^s}\right]=\left[A_x^{(r)}\right][F]\left[A_y^{(s)}\right]^T,\qquad(24)$$

in which subscripts x and y respectively indicate derivative with respect to spatial x and y, and the superscripts (r) and (s) represent the derivative order. For the first-order derivatives, one can use the following relations (Bert and Malik 1996, Zhao *et al.* 2021a)

$$\left[A_x^{(1)}\right]_{in}=\begin{cases}\dfrac{\prod_{\substack{k=1\\k\neq i,n}}^{N_x}(x_i-x_k)}{\prod_{\substack{k=1\\k\neq n}}^{N_x}(x_n-x_k)} & i,n=1,2,...,N_x;i\neq n\\ \sum_{\substack{k=1\\k\neq i}}^{N_x}(x_i-x_k)^{-1} & i=n=1,2,...,N_x\end{cases}\qquad(25)$$

$$\left[A_y^{(1)}\right]_{jm}=\begin{cases}\dfrac{\prod_{\substack{k=1\\k\neq j,m}}^{N_y}(y_i-y_k)}{\prod_{\substack{k=1\\k\neq m}}^{N_x}(y_m-y_k)} & j,m=1,2,...,N_x;j\neq m\\ \sum_{\substack{k=1\\k\neq j}}^{N_y}(y_j-y_k)^{-1} & j=m=1,2,...,N_y\end{cases}$$

and for higher-order ones, the following relation can be employed (Huang *et al.* 2021, Ma *et al.* 2021a)

$$\left[A_x^{(r)}\right]=\left[A_x^{(1)}\right]\left[A_x^{(r-1)}\right],\quad\left[A_y^{(s)}\right]=\left[A_y^{(1)}\right]\left[A_y^{(s-1)}\right].\qquad(26)$$

Utilizing the concepts of the equivalent vector and the Kronecker product ($\otimes$), Eq. (24) can be rewritten as follows (Torabi and Afshari 2017)

$$\left\{\frac{\partial^{r+s}F^*}{\partial x^r\partial y^s}\right\}=\left(\left[A_y^{(s)}\right]\otimes\left[A_x^{(r)}\right]\right)\left\{F^*\right\},\qquad(27)$$

The set of the grid points plays an important role in the convergence of the solution via the DQM. In this paper, a non-uniform distribution pattern which is known as the Chebyshev-Gauss–Lobatto pattern is used, which is defined for $0\le x\le L$ and $0\le y\le b$ as follows (Bert and Malik 1996, Xu *et al.* 2021)

$$x_i=\frac{a}{2}\left\{1-\cos\left[\frac{(i-1)\pi}{N_x-1}\right]\right\},\quad y_i=\frac{b}{2}\left\{1-\cos\left[\frac{(j-1)\pi}{N_y-1}\right]\right\}.\qquad(28)$$

Using Eq. (27), the governing equations (19) can be stated in the following algebraic form

$$[K]\{s\}=\{f\}\qquad(29)$$

in which with the following definition, $[K]$ is stiffness matrix and $\{s\}$ and $\{f\}$ respectively are displacement and external load vectors

$$[K]=\begin{bmatrix}k_{11}&k_{12}&k_{13}\\ k_{21}&k_{22}&k_{23}\\ k_{31}&k_{32}&k_{33}\end{bmatrix},\quad\{s\}=\begin{Bmatrix}\{w^*\}\\ \{\phi^*\}\\ \{\Psi^*\}\end{Bmatrix},\quad\{s\}=\begin{Bmatrix}\{f_1^*\}\\ \{f_2^*\}\\ \{f_3^*\}\end{Bmatrix},\qquad(30)$$

where

$$\begin{aligned}&k_{11}=[z_{11}](I^y\otimes A^x)+[z_{12}](I^y\otimes B^x)+[z_{13}](I^y\otimes C^x)\\ &+[z_{14}](I^y\otimes D^x)\\ &[z_{15}](B^y\otimes A^x)+[z_{16}](B^y\otimes B^x)+[z_{17}](D^y\otimes I^x)\\ &+[z_{18}](B^y\otimes I^x)-k_w(I^y\otimes I^x),\\ &k_{12}=[z_1](I^y\otimes I^x)+[z_2](I^y\otimes A^x)+[z_3](I^y\otimes B^x)\\ &+[z_4](I^y\otimes C^x)+\\ &[z_5](B^y\otimes A^x)+[z_6](B^y\otimes I^x),\\ &k_{13}=[z_7](A^y\otimes I^x)+[z_8](A^y\otimes A^x)+[z_9](A^y\otimes B^x)\\ &+[z_{10}](C^y\otimes I^x),\\ &\{f_1^*\}=vec\{f_1(x_i,y_i\},\end{aligned}$$

$$
\begin{aligned}
&k_{21}=[s_7](I^y\otimes A^x)+[s_8](I^y\otimes B^x)+[s_9](I^y\otimes C^x)\\
&+[s_{10}](B^y\otimes A^x)+[s_{11}](B^y\otimes I^x),\\
&k_{22}=[s_1](I^y\otimes I^x)+[s_2](I^y\otimes A^x)+[s_3](I^y\otimes B^x)\\
&+[s_4](B^y\otimes I^x),\\
&k_{23}=[s_5](A^y\otimes I^x)+[s_6](A^y\otimes A^x)\\
&\left\{f_2^*\right\}=vec\left\{f_2(x_i,y_i\right\},\\
&k_{31}=[r_7](A^y\otimes I^x)+[r_8](A^y\otimes A^x)+[r_9](A^y\otimes B^x)\\
&+[r_{10}](C^y\otimes I^x),\\
&k_{32}=[r_1](A^y\otimes I^x)+[r_2](A^y\otimes A^x),\\
&k_{33}=[r_3](I^y\otimes I^x)+[r_4](I^y\otimes A^x)+[r_5](I^y\otimes B^x)\\
&+[r_6](B^y\otimes I^x)\\
&\left\{f_3^*\right\}=vec\left\{f_3(x_i,y_i\right\},
\end{aligned}
\tag{31}
$$

where "vec" shows the equivalent vector operator and the following diagonal matrices are defined

$$
\begin{aligned}
&[z_k]_{ij}=diag\left\{Z_k(x_i,y_i)\right\},\\
&[s_k]_{ij}=diag\left\{S_k(x_i,y_i)\right\},\\
&[r_k]_{ij}=diag\left\{R_k(x_i,y_i)\right\},
\end{aligned}
\tag{32}
$$

where "diag" provides diagonal matrices.

Similarly, the boundary conditions (21) and (22) can be stated using Eq. (27) in the following algebraic form

$$[T]\{s\}=\{R\}, \tag{33}$$

where $[T]$ and $\{R\}$ can be stated based on the boundary conditions at four edges of the plate.

Eqs. (29) and (33) should be solved simultaneously, which generates an inconsistency between the numbers of unknown variables and the number of algebraic equations (Afshari 2020a, b). In order to overcome this challenge, the grid points should be divided into two sets: The points located at the edges of the plate, which are known as boundary points (denoted by subscript b), and other interior ones, which are known as domain points (denoted by subscript d).

By neglecting satisfying Eq. (29) at the boundary points, the following relation can be obtained

$$[\tilde{K}]\{s\}=\{f\}_d, \tag{34}$$

in which the sign ~ is used to show the non-square matrices.

Eqs. (33) and (34) can be rearranged and partitioned in order to separate the domain and boundary points as follows (Liu *et al*. 2021)

$$[\tilde{K}]_b\{s\}_b+[\tilde{K}]_d\{s\}_d=\{f\}_d, \tag{35a}$$

$$[T]_d\{s\}_d+[T]_b\{s\}_b=\{R\}, \tag{35b}$$

Eq. (35(b)) can be rewritten in the following form

$$\{s\}_b=[T]_b^{-1}\{R\}-[T]_b^{-1}[T]_d\{s\}_d. \tag{36}$$

By substituting Eq. (36) into Eq. (35(a)), the following relation can be obtained

Table 1 Displacement convergence of the center point of the plate (mm) for different boundary conditions

	$N_x=N_y=N$						Percentage difference between N=15 and N=17
	7	9	11	13	15	17	
CCCC	0.6357	0.6438	0.6553	0.6565	0.6582	0.6586	0.06 %
SSSS	1.2526	1.4191	1.4813	1.5034	1.5138	1.5187	0.33 %
CSCS	0.8374	0.8958	0.9245	0.9327	0.9373	0.9392	0.21 %
CCSS	0.8769	0.9343	0.9662	0.9763	0.9819	0.9844	0.25 %

$$[K^*]\{s\}_d=\{f^*\}, \tag{37}$$

where

$$
\begin{aligned}
&[K^*]=[\tilde{K}]_d-[\tilde{K}]_b[T]_b^{-1}[T]_d,\\
&\{f^*\}=\{f\}_d-[\tilde{K}]_b[T]_b^{-1}\{R\}
\end{aligned}
\tag{38}
$$

Solution of the algebraic Eq. (37) provides the displacement vector can be obtained at the domain points, and the corresponding ones at the boundary points can be obtained using Eq. (36). The strain and stress tensor components can be calculated using the received displacement vector.

2. Numerical results

Numerical results are presented in the current section. It is noteworthy that four capital letters are considered to express the boundary condition at x=0, y=0, x=a, and y=b, respectively. Except for the cases which are mentioned directly, results are presented for a CCSS plate subjected to a sinusoidal distributed load $Q(x,y)=10^5\sin\left(\frac{\pi x}{a}\right)\sin\left(\frac{\pi y}{b}\right)\frac{N}{m^2}$.

In Table 1, convergence results are shown with different numbers of grid points (N_x=N_y=N). The results show that convergence is obtained with an increased number of points to the same results. The result difference percentage for the two cases, N=15 and N=17, is negligible. Therefore, convergence in this work is obtained at N=15.

Also, this table indicates that the maximum and minimum deflections respectively belong to SSSS and CCCC plates. Thus, as the supports become more substantial, the stiffness of the plate increases and consequently, its displacement decreases.

Fig. 2 shows the convergence of shear stresses under different boundary conditions. This figure indicates after N=15, the shear stress graphs are matched together, and this match shows the convergence in the presented numerical solution.

The validation of the presented work is performed individually in mechanical and thermal loadings. For a CSCS plate with nonuniform thickness $h(x)=h_0\left[1+\lambda\left(\frac{2x}{a}-1\right)^n\right]$ under the uniform mechanical

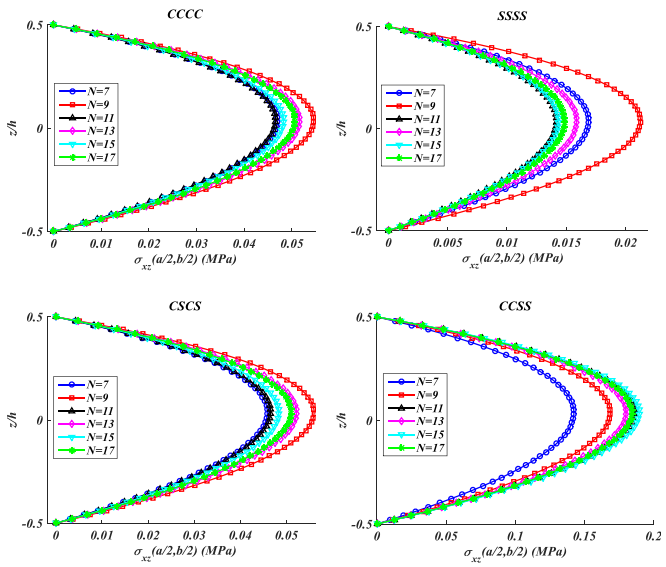

Fig. 2 Convergence of the shear stress (σ_{xz}) at the center point of the plate for different boundary conditions

Table 2 Validation of displacements of the center point of the plate under mechanical load in the presented work

a/b	1	1.1	1.4	1.6	1.8	2	3
Presented	1.5462	2.0607	3.8825	5.1694	6.3920	7.4904	10.8836
Zenkour (2018)	1.5585	2.0756	3.9040	5.1934	6.4173	7.5068	10.8969

load Q. For $h_0/b=0.01$, $\lambda=0.2$, $n=2$ and various values of aspect ratio, the dimensionless deflection of the center point of the plate $w^*=\dfrac{10^3 Eh^3}{12(1-\nu^2)Qb^4}w$ is presented in Table 2 along with those reported by Zenkour (2018). This table confirms that results are in high agreement.

Furthermore, a validation for thermal load is performed based on Navier's solution. The following relations are expressed for SSSS and SCSS plates (Cheng 2018)

$$w(x,y)=\frac{16M^T}{(1-\nu)\pi^4 D}$$

$$\text{SSSS:}\quad \sum_{m=1,3,..}^{\infty}\sum_{n=1,3,..}^{\infty}\frac{\sin\left(\dfrac{m\pi x}{a}\right)\sin\left(\dfrac{n\pi y}{b}\right)}{mn\left[\left(\dfrac{m}{a}\right)^2+\left(\dfrac{n}{b}\right)^2\right]}$$

$$w(x,y)=-\frac{4a^2M^T}{\pi^3 D}\sum_{m=1,3,..}^{\infty}\frac{1}{m^3\cosh\left(\dfrac{m\pi b}{2a}\right)}\cosh\left[\frac{m\pi b}{2a}\left(\frac{2y}{b}-1\right)\right]\sin\left(\frac{m\pi x}{a}\right)-\frac{M^T}{2D}x(x-a)-\frac{8M^T}{\pi^4 Db^2}\sum_{m=1,3,..}^{\infty}\sum_{n=1,3,..}^{\infty}\frac{n}{m\left[\left(\dfrac{m}{a}\right)^2+\left(\dfrac{n}{b}\right)^2\right]}\sin\left(\frac{m\pi x}{a}\right)\sin\left(\frac{n\pi y}{b}\right)\quad (39)$$

$$\text{SCSS:}$$

in which

$$M^T(x,y)=\int_{-\frac{h}{2}}^{\frac{h}{2}}E(z)\alpha(z)\Delta T(z)z\,dz$$
$$\Delta T(z)=T(z)-T_0 \quad (40)$$

The temperature distribution is assumed to be linear as

$$T(z)=\frac{1}{h}\left[\left(\frac{h}{2}-z\right)T_{bot}+\left(\frac{h}{2}+z\right)T_{top}\right] \quad (41)$$

To check the accuracy of the presented work under thermal loadings, a comparison is made between the maximum deflection of this study and the exact solution presented by Cheng (2018) in Figs. 3 and 4. These figures show a high agreement between the results. It is good to note that all material and geometry properties which are used in this validation are expressed in Eq. (5), but it is considered that the plate is homogenous $(C_{\max}=C_{\min}=0)$ and there is no foundation under the plate $(k_w=0)$.

Fig. 5 shows the effect of aspect ratio on the deflection and shear stress σ_{xy}. By increasing the aspect ratio, the flexural stiffness of the plate decreases, and the area of the plate and consequently the extensive load applied on the surface of the plate increases. Thus, as observed in Fig. 5, an increase in the aspect ratio results in a larger deflection. This figure also shows that shear stress σ_{xy} diminishes by increasing the aspect ratio.

Fig. 6 indicates the variation of normal stresses σ_{xx} and σ_{yy} for various values of aspect ratio (b/a). This figure

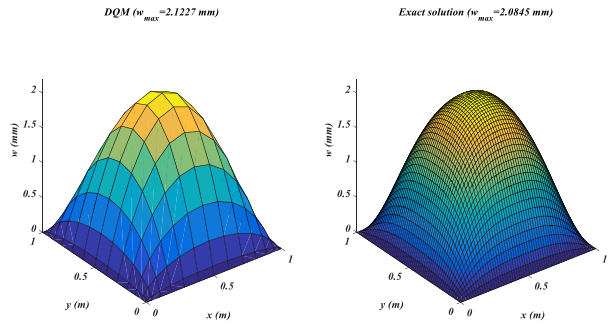

Fig. 3 Deflection of the SSSS plate under thermal loading

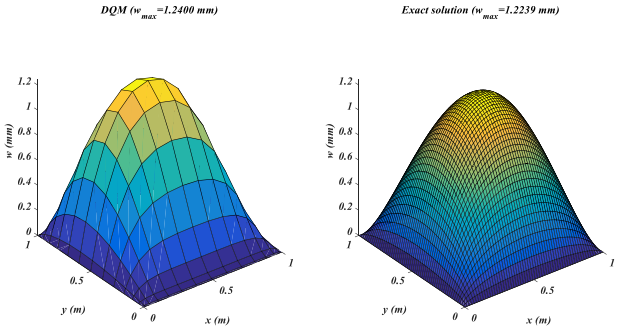

Fig. 4 Deflection of the SCSS plate under thermal loading

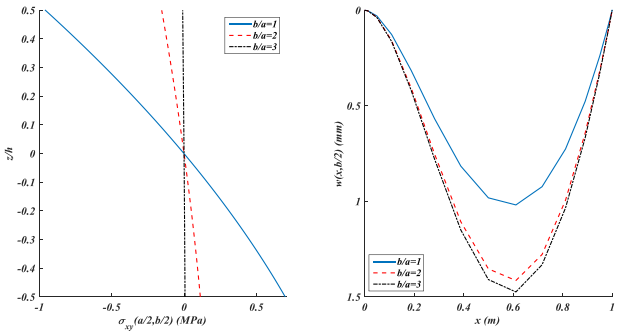

Fig. 5 Variation of shear stress and deflection for various values of aspect ratio

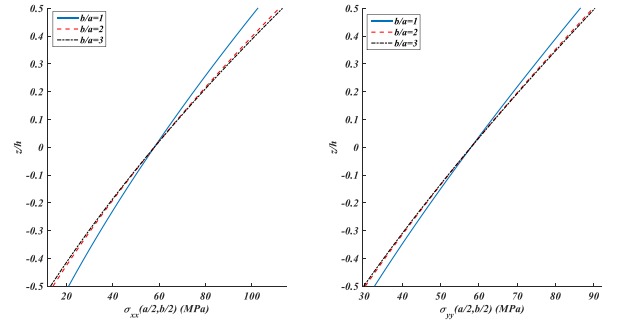

Fig. 6 Variation of normal stresses for various values of aspect ratio

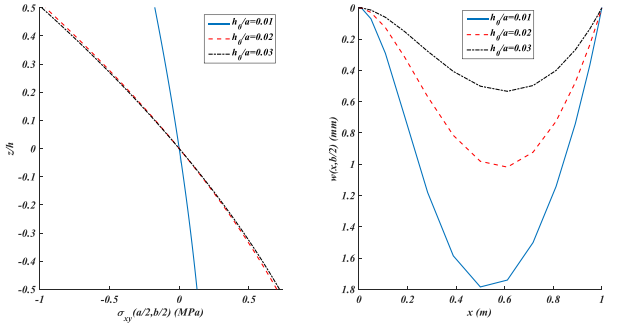

Fig. 7 Variation of shear stress and deflection for various values of the thickness-to-length ratio

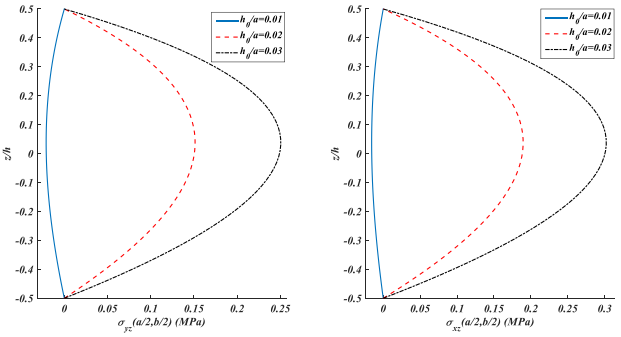

Fig. 8 Variation of shear stresses for various values of the thickness-to-length ratio

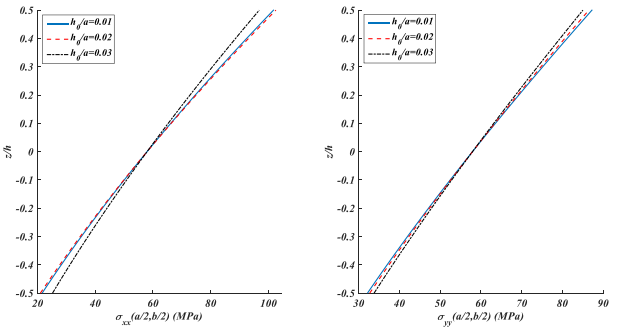

Fig. 9 Variation of the normal stresses for various values of the thickness-to-length ratio

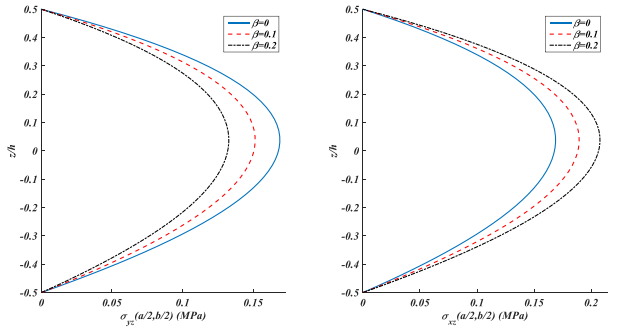

Fig. 10 Variation of shear stresses for various values of the thickness variation parameter β

shows that the effect of the aspect ratio on normal stress is not extensive.

Fig. 7 shows the variation of shear stress σ_{xy} and deflection for various values of the thickness-to-length ratio (h_0/a). As observed, a reduction in deflection occurs with an increase in the value of the thickness to length ratio h_0/a because of increasing the stiffness of the plate. This figure also shows that shear stress σ_{xy} increases by increasing the thickness-to-length ratio.

Fig. 8 indicates the variation of shear stresses σ_{xz} and σ_{yz} for various values of the thickness-to-length ratio (h_0/a). As shown in this figure, an increase in the thickness results in an increase in shear stresses. Thus, for thick plates, it is essential to incorporate the shear stress and use more substantial theories like the TDST.

Fig. 9 shows the variation of normal stresses σ_{xx} and σ_{yy} for various values of thickness-to-length ratio (h_0/a). As this figure shows, the thickness-to-length ratio does not significantly affect the normal stresses.

The effect of the thickness variation parameter β on the shear stresses σ_{xz} and σ_{yz} is studied in Fig. 10. As shown in this figure, by increasing the thickness variation parameter β, shear stresses σ_{yz} decreases but shear stresses σ_{xz} grows.

Figs. 11-13 investigate the variation of stress components and deflection for various values of $C_{\min}$. As shown in Fig. 11, an increase in $C_{\min}$ leads to a rise in

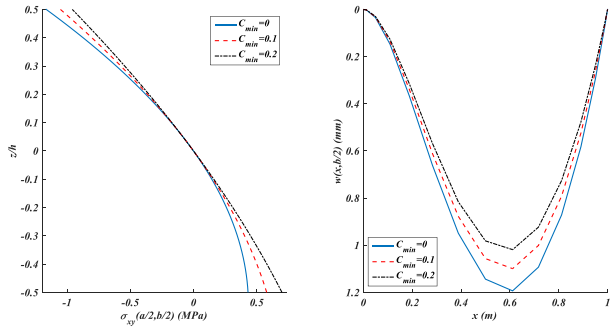

Fig. 11 Variation of shear stress and deflection for various values of $C_{\min}$

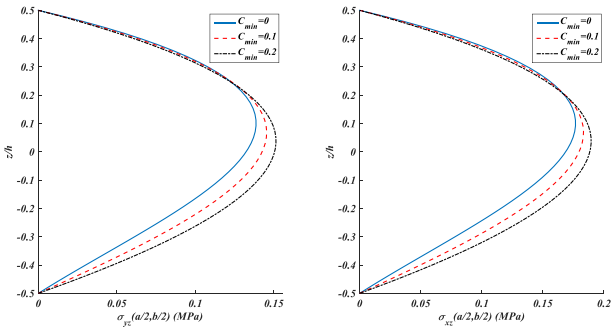

Fig. 12 variation of shear stresses for various values of $C_{\min}$

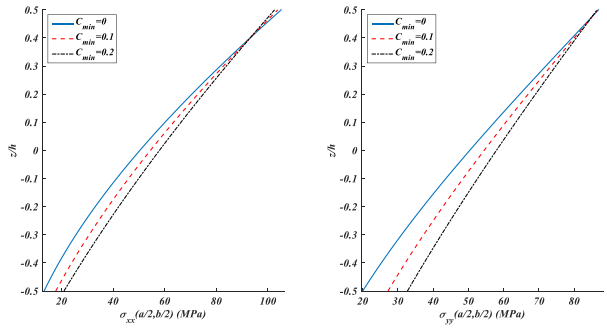

Fig. 13 Variation of normal stresses for various values of $C_{\min}$

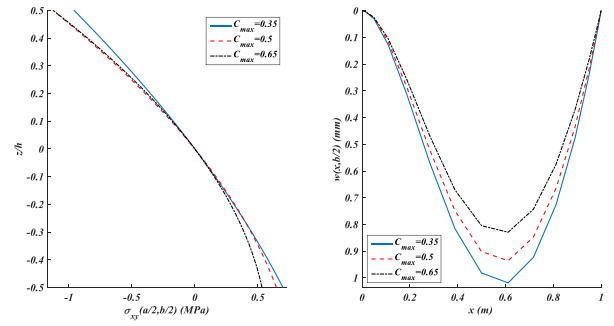

Fig. 14 Variation of shear stress and deflection for various values of $C_{\max}$

stiffness and, consequently, a decrease in deflection. Figs. 12 and 13 show that shear stresses σ_{xz} and σ_{yz}, normal stresses σ_{xx} and σ_{yy} grow by increasing $C_{\min}$.

Figs. 14-16 indicate the variation of stress components and deflection for various values of $C_{\max}$. Fig. 14 shows that an increase in $C_{\max}$ leads to an increase in stiffness and a reduction in deflection. Figs. 15 and 16 show that no specific trend can be found for the variation of stress components by the variation of $C_{\max}$.

The effects of the elastic foundation on the deflection and stress components are studied in Figs. 17-19. As shown in these figures, a decrease in shear stresses and deflection is observed with an increase in the stiffness coefficient of the foundation.

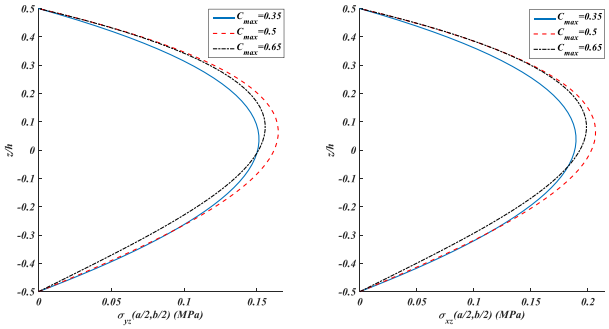

Fig. 15 variation of shear stresses for various values of $C_{\max}$

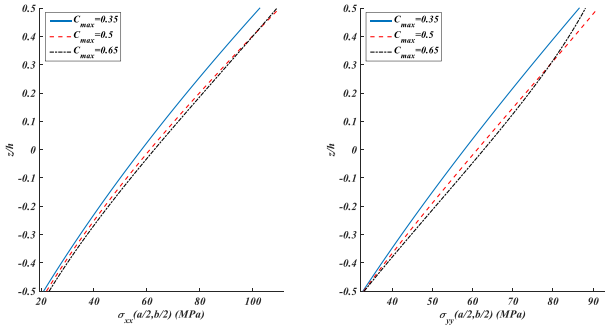

Fig. 16 Variation of normal stresses for various values of $C_{\max}$

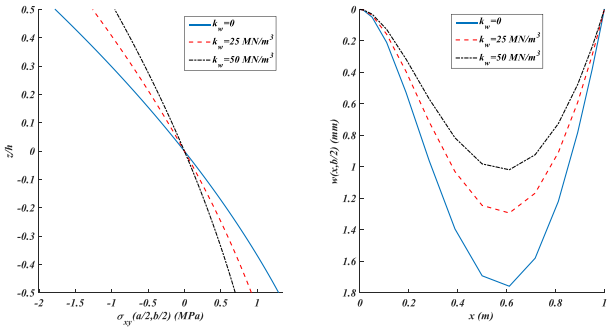

Fig. 17 Variation of shear stress and deflection for various values of the foundation's parameter

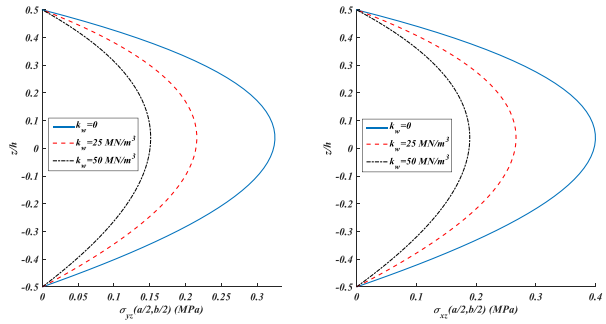

Fig. 18 Variation of shear stresses for various values of foundation's parameter

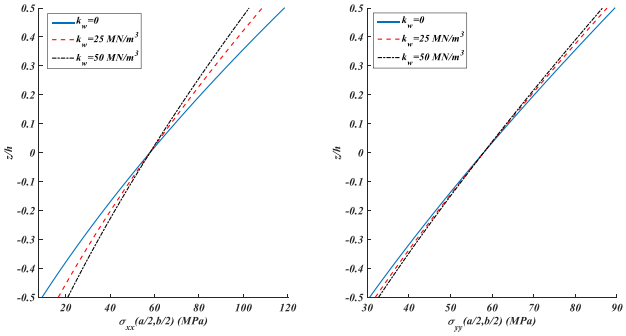

Fig. 19 Variation of normal stresses for various values of foundation's parameter

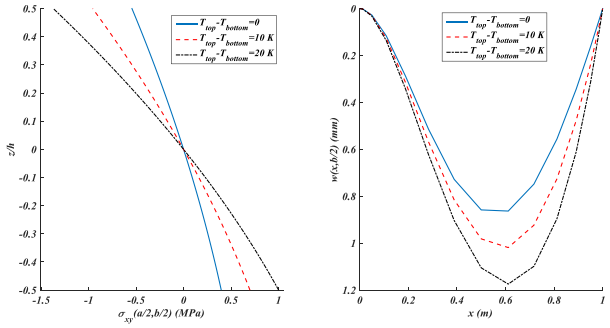

Fig. 20 Variation of shear stress and deflection for various values of $T_{top}-T_{bottom}$

Figs. 20-22 investigate the effect of top and bottom surfaces temperature differences on the variation of shear and normal stresses and deflection of the plate. In this case, the temperature of the bottom surface is considered to be constant and temperature of the top surface is variable. Fig. 20 indicates the variation of shear stress σ_{xy} and deflection for various values of temperature differences ($T_{top}-T_{bottom}$). This figure shows that an increase in temperature difference leads to an increase in deflection. Fig. 21 shows the changes of shear stresses σ_{xz} and σ_{yz} for various temperature difference values ($T_{top}-T_{bottom}$). According to this figure, an increase in shear stresses and deflection is observed with an increase in the temperature

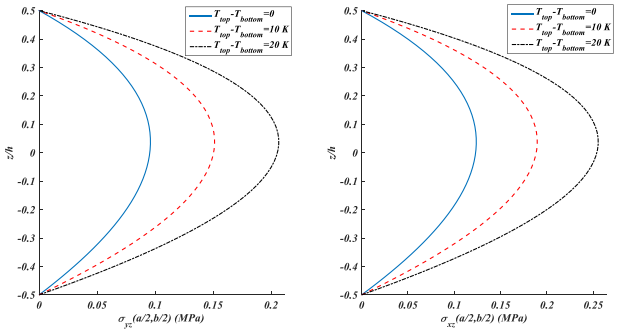

Fig. 21 Changes of shear stresses for various values of $T_{top}-T_{bottom}$

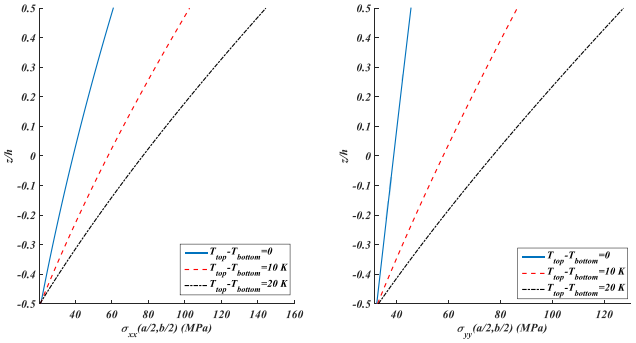

Fig. 22 Variation of normal stresses for various values of $T_{top}-T_{bottom}$

difference. Fig. 22 shows the variation of normal stresses σ_{xx} and for various temperature difference ($T_{top}-T_{bottom}$). As observed, normal stresses grow by increasing the temperature difference.

5. Conclusions

This paper presented a thermoelastic analysis of variable thickness plates made of FGMs resting on an elastic foundation and subjected to mechanical and thermal loads. The thermal load was applied to the plate as a temperature difference between the top and bottom surfaces of the plate. Temperature distribution in the plate was obtained using the steady-state heat equation. Except for Poisson's ratio, all mechanical properties were assumed to be variable along the thickness direction based on the volume fractions of ceramic and metal. The main results of the presented paper are as follows:

By increasing the aspect ratio, the deflection of the plate rises.

Increasing the temperature difference (when the bottom surface temperature is constant the top surface increases) increases deflection of the plate and stress components.

An elastic foundation reduces deflection and stress components.

By increasing the volume fraction of Silicon Carbide at the bottom surface of the plate (Cmin), a decrease in deflection and an increase in stress components is apparent.

By increasing the volume fraction of Silicon Carbide at the top surface of the plate (Cmax), deflection of the plate decreases. But, no specific trend can be seen for the variation of stress components.

An increase in the thickness causes an increase in shear stress and reduces the deflection of the plate.

The most influential parameter on the normal stresses is the temperature difference between the top and bottom surfaces.

A reduction in shear stresses and deflection is observed by increasing the stiffness coefficient of the foundation**.**

References

Adab, N. and Arefi, M. (2022), "Vibrational behavior of truncated conical porous GPL-reinforced sandwich micro/nano-shells", *Eng. Comput*., 1-25. https://doi.org/10.1007/s00366-021-01580-8.

Adab, N., Arefi, M. and Amabili, M. (2022), "A comprehensive vibration analysis of rotating truncated sandwich conical microshells including porous core and GPL-reinforced face-sheets", *Compos. Struct.*, **279**, 114761. https://doi.org/10.1016/j.compstruct.2021.114761.

Arefi, M., Rahimi, G.H. and Khoshgoftar, M.J. (2011), "Optimized design of a cylinder under mechanical, magnetic and thermal loads as a sensor or actuator using a functionally graded piezomagnetic material", *Int. J. Phys. Sci.*, **6**(27), 6315-6322. https://doi.org/10.5897/IJPS10.597.

Arefi, M. and Rahimi, G.H. (2011), "Non linear analysis of a functionally graded square plate with two smart layers as sensor and actuator under normal pressure", *Smart. Struct. Syst.*, **8**(5), 433-447. https://doi.org/10.12989/sss.2011.8.5.433.

Arefi, M. and Rahimi, G.H. (2012), "Studying the nonlinear behavior of the functionally graded annular plates with piezoelectric layers as a sensor and actuator under normal pressure", *Smart. Struct. Syst.*, **9**(2), 127-143. https://doi.org/10.12989/sss.2012.9.2.127.

Arefi, M. Nahas, I. (2014), "Nonlinear electro thermo elastic analysis of a thick spherical functionally graded piezoelectric shell", *Compos. Struct.* **118**, 510-518. 10.1016/j.compstruct.2014.08.002

Arefi, M. and Rahimi, G.H. (2014), "Application of shear deformation theory for two dimensional electro-elastic analysis of a FGP cylinder", *Smart. Struct. Syst.*, **13**(1), 1-24. https://doi.org/10.12989/sss.2014.13.1.001.

Arefi, M., Mohammadi, M., Tabatabaeian, A., Dimitri, R. and Tornabene, F. (2018), "Two-dimensional thermo-elastic analysis of FG-CNTRC cylindrical pressure vessels", *Steel. Compos. Struct*., **27**(4), 525-536. https://doi.org/10.12989/scs.2018.27.4.525.

Arefi, M. (2014), "A complete set of equations for piezo-magnetoelastic analysis of a functionally graded thick shell of revolution", *Lat. Amer. J. Solids. Struct*., **11**(11), 2073-2092. https://doi.org/10.1590/S1679-78252014001100009.

Afshari, H. (2020a), "Effect of graphene nanoplatelet reinforcements on the dynamics of rotating truncated conical shells", *J. Braz. Soc. Mech. Sci. Eng.*, **42**(10), 1-22. https://doi.org/10.1007/s40430-020-02599-6.

Afshari, H. (2020b), "Free vibration analysis of GNP-reinforced truncated conical shells with different boundary conditions", *Austr. J. Mech. Eng.*, 1-17. https://doi.org/10.1080/14484846.2020.1797340.

Ahmadi, H. and Foroutan, K. (2019), "Combination resonance analysis of FG porous cylindrical shell under two-term excitation", *Steel. Compos. Struct*., **32**(2), 253-264. https://doi.org/10.12989/scs.2019.32.2.253.

Al-Furjan, M.S.H., Habibi, M., Rahimi, A., Chen, G., Safarpour, H., Safarpour, M. and Tounsi, A. (2020a), "Chaotic simulation of the multi-phase reinforced thermo-elastic disk using GDQM", *Eng. Comput.*, 1-24. https://doi.org/10.1007/s00366-020-01144-2.

Al-Furjan, M.S.H., Habibi, M., Ni, J. and Tounsi, A. (2020b), "Frequency simulation of viscoelastic multi-phase reinforced fully symmetric systems", *Eng. Comput.*, 1-17. https://doi.org/10.1007/s00366-020-01200-x.

Al-Furjan, M., Safarpour, H., Habibi, M., Safarpour, M. and Tounsi, A. (2020), "A comprehensive computational approach for nonlinear thermal instability of the electrically FG-GPLRC disk based on GDQ method", *Eng. Comput.*, 1-18. https://doi.org/10.1007/s00366-020-01088-7.

Ali, A., Zhang, C., Bibi, T., Zhu, L., Cao, L., Li, C. and Hsiao, P. (2022). "Investigation of five different low-cost locally available isolation layer materials used in sliding base isolation systems". *Soil Dyn. Earthq. Eng*., **154**, 107127. https://doi.org/10.1016/j.soildyn.2021.107127.

Bai, Y., Alzahrani, B., Baharom, S. and Habibi, M. (2020), "Semi-numerical simulation for vibrational responses of the viscoelastic imperfect annular system with honeycomb core under residual pressure", *Eng. Comput.*, 1-26. https://doi.org/10.1007/s00366-020-01191-9.

Barati, M.R. (2017), "Vibration analysis of FG nanoplates with nanovoids on viscoelastic substrate under hygro-thermo-mechanical loading using nonlocal strain gradient theory", *Struct. Eng. Mech.*, **64**(6), 683-693. https://doi.org/10.12989/sem.2017.64.6.683.

Beena, K.P. and Parvathy, U. (2014), "Linear static analysis of functionally graded plate using spline finite strip method", *Compos. Struct*., **117**, 309-315. https://doi.org/10.1016/j.compstruct.2014.07.002.

Bellifa, H., Selim, M.M., Chikh, A., Bousahla, A.A., Bourada, F., Tounsi, A., Benrahou, K.H., Al-Zahrani, M.M. and Tounsi A. (2021), "Influence of porosity on thermal buckling behavior of functionally graded beams", *Smart. Struct. Syst*., **27**(4), 719-728. https://doi.org/10.12989/sss.2021.27.4.719.

Bellman, R., Kashef, B.J. and Casti, J. (1972), "Differential quadrature: a technique for the rapid solution of nonlinear partial differential equations", *J. Comput. Phys*., **10**(1), 40-52. https://doi.org/10.1016/0021-9991(72)90089-7.

Bert, C.W. and Malikm, M. (1996), "Differential quadrature method in computational mechanics: a review", *Appl. Mech. Rev*., **49**(1), 1-28. https://doi.org/10.1115/1.3101882.

Brischetto, S., Leetsch, R., Carrera, E., Wallmersperger, T. and Kröplin, B. (2008), "Thermo-mechanical bending of functionally graded plates", *J. Therm. Stresses*, **31**(3), 286-308. https://doi.org/10.1080/01495730701876775.

Carrera, E. (2002), "Theories and finite elements for multilayered, anisotropic, composite plates and shells", *Arch. Comput. Meth. Eng.*, **9**(2), 87-140. https://doi.org/10.1007/BF02736649.

Casmed, C.A., Gordon, F., Bernard, K.A. and Sylvester, A. (2021), "Geostatistical approach for the estimation of shear-hosted gold deposit: A case study of the Obuasi gold deposit, Ghana". *Malays. J. Geosci*., **5**(2), 76-84.

Chen, F., Jin, Z., Wang, E., Wang, L., Jiang, Y., Guo, P., Gao, S. and He, X. (2021), "Relationship model between surface strain of concrete and expansion force of reinforcement rust". *Sci. Rep.*, **11**, 4208. https://doi.org/10.1038/s41598-021-83376-w.

Cheng, Z.Q. and Batra, R.C. (2000), "Deflection relationships between the homogeneous Kirchhoff plate theory and different functionally graded plate theories", *Arch. Mech.*, **52**(1), 143-158.

Cheng, X. (2018), *Thermal Elastic Mechanics Problems of Concrete Rectangular Thin Plate*, Springer Tracts in Civil Engineering, Mainland, China.

Ching, H.K. and Yen, S.C. (2005), "Meshless local Petrov-Galerkin analysis for 2D functionally graded elastic solids under mechanical and thermal loads", *Compos. B: Eng.*, **36**(3), 223-240. https://doi.org/10.1016/j.compositesb.2004.09.007.

Chung, Y.L. and Chen, W.T. (2007), "The flexibility of functionally graded material plates subjected to uniform loads", *J. Mech. Mater. Struct.*, **2**(1), 63-86. https://doi.org/10.2140/jomms.2007.2.63.

Chu, Y.M. Shankaralingappa, B.M., Gireesha, B.J., Alzahrani, F., Ijaz Khan, M. and Khan, S.U. (2021), "Combined impact of Cattaneo-Christov double diffusion and radiative heat flux on bio-convective flow of Maxwell liquid configured by a stretched nano-material surface", *Appl. Math. Comput.*, https://doi.org/10.1016/j.amc.2021.126883.

Chu, Y.M. Nazir, U., Sohail, M., Selim, M.M. and Lee, J.R. (2021), "Enhancement in thermal energy and solute particles using hybrid nanoparticles by engaging activation energy and chemical reaction over a parabolic surface via finite element approach", *Fractal. Fract.*, **5**(3), Article 119, 17 pages. https://doi.org/10.3390/fractalfract5030119.

Dai, Z., Jiang, Z., Zhang, L. and Habibi, M. (2021), "Frequency characteristics and sensitivity analysis of a size-dependent laminated nanoshell", *Adv. Nano. Res.*, **10**(2), 175-189. https://doi.org/10.12989/anr.2021.10.2.175.

Dai, Z., Zhang, L., Bolandi, S.Y. and Habibi, M. (2021), "On the vibrations of the non-polynomial viscoelastic composite open-type shell under residual stresses", *Compos. Struct.*, **263**, 113599. https://doi.org/10.1016/j.compstruct.2021.113599.

Ghorbanpour Arani, A., Kiani, F. and Afshari, H. (2019), "Aeroelastic analysis of laminated FG-CNTRC cylindrical panels under yawed supersonic flow", *Int. J. Appl. Mech.*, **11**(6), 1950052. https://doi.org/10.1142/S1758825119500522.

Ghorbanpour Arani, A., Kiani, F. and Afshari, H. (2021), "Free and forced vibration analysis of laminated functionally graded CNT-reinforced composite cylindrical panels", *J. Sandw. Struct. Mater.*, **23**(1), 255-278. https://doi.org/10.1177/1099636219830787.

Golmakaniyoon, S. and Akhlaghi, F. (2016), "Time-dependent creep behavior of Al–SiC functionally graded beams under in-plane thermal loading", *Comput. Mater. Sci.*, **121**, 182-190. https://doi.org/10.1016/j.commatsci.2016.04.038.

Heidari, Y., Arefi, M. and Irani-Rahaghi, M. (2021), "Free vibration analysis of cylindrical micro/nano-shell reinforced with CNTRC patches", *Int. J. Appl. Mech.*, **13**(4), 2150040.

Hajiseyedazizi, S.N., Samei, M.E., Alzabut, J. and Chu, Y.M. (2021), "On multi-step methods for singular fractional q-integro-differential equations", *Open. Math.*, **19**, 1-28. https://doi.org/10.1515/math-2021-0093

Habibi, M., Darabi, R., Sa, J.C.D. and Reis, A. (2021), "An innovation in finite element simulation via crystal plasticity assessment of grain morphology effect on sheet metal formability", *Proc. the Inst. Mech. Eng., Part L: J. Mater: Design. Appl.*, **235**(8), 1937-1951. https://doi.org/10.1177/14644207211024686.

Hosseini-Hashemi, S. and Khaniki, H.B. (2018), "Three dimensional dynamic response of functionally graded nanoplates under a moving load", *Struct. Eng. Mech.*, **66**(2), 249-262. https://doi.org/10.12989/sem.2018.66.2.249.

Huang, X., Hao, H., Oslub, K., Habibi, M. and Tounsi, A. (2021), "Dynamic stability/instability simulation of the rotary size-dependent functionally graded microsystem", *Eng. Comput.*, 1-17. https://doi.org/10.1007/s00366-021-01399-3.

Huang, X., Zhang, Y., Moradi, Z. and Shafiei, N. (2021), "Computer simulation via a couple of homotopy perturbation methods and the generalized differential quadrature method for nonlinear vibration of functionally graded non-uniform micro-tube", *Eng. Comput.*, 1-18. https://doi.org/10.1007/s00366-021-01395-7.

Huang, X., Zhu, Y., Vafaei, P., Moradi, Z. and Davoudi, M. (2021), "An iterative simulation algorithm for large oscillation of the applicable 2D-electrical system on a complex nonlinear substrate", *Eng. Comput.*, 1-13. https://doi.org/10.1007/s00366-021-01320-y.

Huang, K., Su, B., Li, T., Ke, H., Lin, M. and Wang, Q. (2022). "Numerical simulation of the mixing behaviour of hot and cold fluids in the rectangular T-junction with/without an impeller". *Appl. Therm. Eng.*, **204**, 117942. https://doi.org/10.1016/j.applthermaleng.2021.117942.

Huo, J., Zhang, G., Ghabussi, A. and Habibi, M. (2021), "Bending analysis of FG-GPLRC axisymmetric circular/annular sector plates by considering elastic foundation and horizontal friction force using 3D-poroelasticity theory", *Compos. Struct.*, **276**, 114438. https://doi.org/10.1016/j.compstruct.2021.114438.

Iqbal, M.A., Wang, Y., Miah, M.M. and Osman, M.S. (2022), "Study on date–Jimbo–Kashiwara–Miwa equation with conformable derivative dependent on time parameter to find the exact dynamic wave solutions", *Fractal. Fract.*, **6**(1), Article 4. https://doi.org/10.3390/fractalfract6010004.

Jia, D., Li, C., Zhang, D., Zhang, Y. and Zhang, X. (2014), "Experimental verification of nanoparticle jet minimum quantity lubrication effectiveness in grinding", *J. Nanoparticle. Res.*, **16**(12), 1-15.

Jin, F., Qian, Z.S., Chu, Y.M. and Rahman, M. ur (2022), "On nonlinear evolution model for drinking behavior under Caputo-Fabrizio derivative", *J. Appl. Anal. Comput.*, https://doi.org/10.11948/20210357.

Kiani, K., Gharebaghi, S. A. and Mehri, B. (2017), "In-plane and out-of-plane waves in nanoplates immersed in bidirectional magnetic fields", *Struct. Eng. Mech.*, **61**(1), 65-76. https://doi.org/10.12989/sem.2017.61.1.065.

Khoshgoftar, M., Rahimi, M.J. and Arefi, G.H. (2013), "Exact solution of functionally graded thick cylinder with finite length under longitudinally non-uniform pressure", *Mech. Res. Com.*, **51**, 61-66. https://doi.org/10.1016/j.mechrescom.2013.05.001.

Kholdi, M., Rahimi, G., Loghman, A., Ashrafi, H. and Arefi, M. (2022), "Analysis of thick-walled spherical shells subjected to various temperature gradients: Thermo-elasto-plastic and residual stress studies", *Int. J. Appl. Mech.*, 2150105.

Li, X., Ding, H. and Chen, W. (2008), "Elasticity solutions for a transversely isotropic functionally graded circular plate subject to an axisymmetric transverse load qr^k", *Int. J. Solids. Struct.*, **45**(1), 191-210. https://doi.org/10.1016/j.ijsolstr.2007.07.023.

Li, J., Xu, K., Chaudhuri, S., Yumer, E., Zhang, H. and Guibas, L. (2017). "GRASS: generative recursive autoencoders for shape structures". *ACM Transac. on Fraph.*, **36**(4), 1-14. https://doi.org/10.1145/3072959.3073637

Liu, Y., Wang, W.,He, T., Moradi, Z. and Benítez, M.A.L. (2021a), "On the modelling of the vibration behaviors viadiscrete singular convolution method forahigh-order sector annular system", *Eng. Comput.*, https://doi.org/10.1007/s00366-021-01454-z.

Liu, Z., Wu, X., Yu, M., and Habibi, M. (2020), "Large-amplitude dynamical behavior of multilayer graphene platelets reinforced nanocomposite annular plate under thermo-mechanical loadings", *Mech. Based. Des. Struct.*, 1-25. https://doi.org/10.1080/15397734.2020.1815544.

Liu, Z., Su, S., Xi, D. and Habibi, M. (2020), "Vibrational responses of a MHC viscoelastic thick annular plate in thermal environment using GDQ method", *Mech. Based. Des. Struct.*, 1-26. https://doi.org/10.1080/15397734.2020.1784201.

Liu, C., Zhao, Y., Wang, Y., Zhang, T. and Jia, H. (2021b), "Hybrid dynamic modeling and analysis of high-speed thin-rimmed gears", *ASME. J. Mech. Des.*, **143**(12): 123401. https://doi.org/10.1115/1.4051137.

Lu, N., Wang, H., Wang, K., & Liu, Y. (2021). "Maximum probabilistic and dynamic traffic load effects on short-to-medium span bridges", *Cmes-Comput. Model. Eng. Sci.*, **127**(1), 345-360. https://doi.org/10.32604/cmes.2021.013792.

Lu, C., Lim, C.W. and Chen, W. (2009), "Semi-analytical analysis for multi-directional functionally graded plates:3-D elasticity solutions", *Int. J. Numer. Meth. Eng.*, **79**(1), 25-44. https://doi.org/10.1002/nme.2555.

Ma, L., Liu, X. and Moradi, Z. (2021), "On the chaotic behavior of graphene-reinforced annular systems under harmonic excitation", *Eng. Comput.*, 1-25. https://doi.org/10.1007/s00366-020-01210-9.

Ma, L. and Wang, T. (2004), "Relationships between axisymmetric bending and buckling solutions of FGM circular plates based on third-order plate theory and classical plate theory", *Int. J. Solids. Struct.*, **41**(1), 85-101. https://doi.org/10.1016/j.ijsolstr.2003.09.008.

Matouk, H., Bousahla, A.A., Heireche, H., Bourada, F., Bedia, E., Tounsi, A. and Benrahou, K.H. (2020), "Investigation on hygro-thermal vibration of P-FG and symmetric S-FG nanobeam using integral Timoshenko beam theory", *Adv. Nano. Res.*, **8**(4), 293-305. https://doi.org/10.12989/anr.2020.8.4.293.

Merazka, B., Bouhadra, A., Menasria, A., Selim, M.M., Bousahla, A.A., Bourada, F., Tounsi, A., Benrahou, K.H. and Al-Zahrani, M.M. (2021), "Hygro-thermo-mechanical bending response of FG plates resting on elastic foundations", *Steel. Compos. Struct.*, **39**(5), 631-643. https://doi.org/10.12989/scs.2021.39.5.631.

Moradi, Z., Davoudi, M., Ebrahimi, F. and Ehyaei, A.F. (2021), "Intelligent wave dispersion control of an inhomogeneous micro-shell using a proportional-derivative smart controller", *Waves. Rand. Complex. Media*, 1-24. https://doi.org/10.1080/17455030.2021.1926572.

Mou, B. and Bai, Y. (2018). "Experimental investigation on shear behavior of steel beam-to-CFST column connections with irregular panel zone". *Eng. Struct.*, **168**, 487-504. https://doi.org/10.1016/j.engstruct.2018.04.029.

Mudhaffar, I.M., Tounsi, A., Chikh, A., Al-Osta, M.A., Al-Zahrani, M.M. and Al-Dulaijan, S.U. (2021), "Hygro-thermo-mechanical bending behavior of advanced functionally graded ceramic metal plate resting on a viscoelastic foundation", *Struct*., https://doi.org/10.1016/j.istruc.2021.05.090.

Najaafi, N., Jamali, M., Habibi, M., Sadeghi, S., Jung, D.W. and Nabipour, N. (2021), "Dynamic instability responses of the substructure living biological cells in the cytoplasm environment using stress-strain size-dependent theory", *J. Biomolec. Struct. Dyn.*, **39**(7), 2543-2554. https://doi.org/10.1080/07391102.2020.1751297.

Nasution, M.K., Syah, R., Ramdan, D., Afshari, H., Amirabadi, H., Selim, M.M., Khan, A., Rahman, M.L. Sarjadi, M.S. and Su, C.H. (2022), "Modeling and computational simulation for supersonic flutter prediction of polymer/GNP/fiber laminated composite joined conical-conical shells", *Arab. J. Chem.*, **15**(1), 103460. https://doi.org/10.1016/j.arabjc.2021.103460.

Nazeer, M., Hussain, F., Ijaz Khan, M., Asad-ur-Rehman, El-Zahar, E.R., Chu, Y.M. and Malik, M.Y. (2021), "Theoretical study of MHD electro-osmotically flow of third-grade fluid in micro channel", *Appl. Math. Comput.*, **420**, https://doi.org/10.1016/j.amc.2021.126868.

Nie, G. and Zhong, Z. (2007), "Semi-analytical solution for three-dimensional vibration of functionally graded circular plates", *Comput. Meth. Appl. Mech. Eng*., **196**(49-52), 4901-4910. https://doi.org/10.1016/j.cma.2007.06.028.

Qiao, W., Li, Z., Liu, W. and Liu, E. (2022), "Fastest-growing source prediction of US electricity production based on a novel hybrid model using wavelet transform", I*nt. J. Energy. Res*., **46**(2), 1766-1788. https://doi.org/10.1002/er.7293

Qiao, W., Wang, Y., Zhang, J., Tian, W., Tian, Y. and Yang, Q. (2021), "An innovative coupled model in view of wavelet transform for predicting short-term PM10 concentration", *J. Environ. Manag.*, **289**, 112438. https://doi.org/10.1016/j.jenvman.2021.112438.

Reddy, J.N. (2007), *Theory and Analysis of Elastic Plates and Shells*, Taylor & Francis, Boca Raton, Florida, United States.

Reddy, J., Wang, C. and Kitipornchai, S. (1999), "Axisymmetric bending of functionally graded circular and annular plates", *Eur. J. Mech.-A/Solids*, **18**(2), 185-199. https://doi.org/10.1016/S0997-7538(99)80011-4.

Refrafi, S., Bousahla, A.A., Bouhadra, A., Menasria, A., Bourada, F., Tounsi, A., Bedia, E.A., Mahmoud, S., Benrahou, K.H. and Tounsi, A. (2020), "Effects of hygro-thermo-mechanical conditions on the buckling of FG sandwich plates resting on elastic foundations", *Comput. Concrete*, **25**(4), 311-325. https://doi.org/10.12989/cac.2020.25.4.311.

Rashid, S., Sultana, S., Karaca, Y., Khalid, A. and Chu, Y.M. (2022a), "Some further extensions considering discrete proportional fractional operators", *Fractals*, **30**(1), 2240026. https://10.1142/S0218348X22400266.

Rashid, S., Abouelmagd, E.I., Khalid, A., Farooq, F.B. and Chu, Y.M. (2022b), "Some recent developments on dynamical $\hbar$-discrete fractional type inequalities in the frame of nonsingular and nonlocal kernels", *Fractals*, **30**(2), 2240110. https://10.1142/S0218348X22401107.

Shao, Y., Zhao, Y., Gao, J. and Habibi, M. (2021), "Energy absorption of the strengthened viscoelastic multi-curved composite panel under friction force", *Arch. Civil. Mech. Eng*., **21**(4), 1-29. https://doi.org/10.1007/s43452-021-00279-3.

Shi, X., Li, J. and Habibi, M. (2020), "On the statics and dynamics of an electro-thermo-mechanically porous GPLRC nanoshell conveying fluid flow", *Mech. Based. Des. Struct.*, 1-37. https://doi.org/10.1080/15397734.2020.1772088.

Sobhy, M. (2017), "Hygro-thermo-mechanical vibration and buckling of exponentially graded nanoplates resting on elastic foundations via nonlocal elasticity theory", *Struct. Eng. Mech*., **63**(3), 401-415. https://doi.org/10.12989/sem.2017.63.3.401.

Song, Y.Q., Zhao, T.H., Chu, Y.M. and Zhang, X.H. (2015), "Optimal evaluation of a Toader-type mean by power mean", *J. Inequal. Appl.*, **408**. https://doi.org/10.1186/s13660-015-0927-6.

Tahir, S.I., Chikh, A., Tounsi, A., Al-Osta, M.A., Al-Dulaijan, S. U. and Al-Zahrani, M.M. (2021), "Wave propagation analysis of a ceramic-metal functionally graded sandwich plate with different porosity distributions in a hygro-thermal environment", *Compos. Struct.*, **269**, 114030. https://doi.org/10.1016/j.compstruct.2021.114030.

Torabi, K. and Afshari, H. (2017), "Optimization for flutter boundaries of cantilevered trapezoidal thick plates", *J. Braz. Soc. Mech. Sci. Eng.*, **39**(5), 1545-1561. https://doi.org/10.1177/1099636217697492.

Tounsi, A., Al-Dulaijan, S., Al-Osta, M.A., Chikh, A., Al-Zahrani, M., Sharif, A. and Tounsi, A. (2020), "A four variable trigonometric integral plate theory for hygro-thermo-mechanical bending analysis of AFG ceramic-metal plates resting on a two-parameter elastic foundation", *Steel. Compos. Struct*., **34**(4)**,** 511-524. https://doi.org/10.12989/scs.2020.34.4.511.

Wang, F.Z., Khan, M.N., Ahmad, I., Ahmad, H., Abu-Zinadah, H. and Chu, Y.M. (2022a), "Numerical solution of traveling waves in chemical kinetics: time-fractional fishers equations", *Fractals*, **30**(2), 22400051, https://10.1142/S0218348X22400515.

Wang, Z., Yu, S., Xiao, Z. and Habibi, M. (2020), "Frequency and buckling responses of a high-speed rotating fiber metal laminated cantilevered microdisk", *Mech. Adv. Mater. Struct.*, 1-14. https://doi.org/10.1080/15376494.2020.1824284.

Wang, K., Wang, H. and Li, S. (2022b). "Renewable quantile regression for streaming datasets". *Knowledge-based Syst.*, **235**, 107675. https://doi.org/10.1016/j.knosys.2021.107675.

Wang, M.K., Hong, M.Y., Xu, Y.F., Shen, Z.H. and Chu, Y.M. (2020), "Inequalities for generalized trigonometric and hyperbolic functions with one parameter", *J. Math. Inequal.*, **14**(1), 1-21. https://dx.doi.org/10.7153/jmi-2020-14-01.

Wei, J., Xie, Z., Zhang, W., Luo, X., Yang, Y. and Chen, B. (2021), "Experimental study on circular steel tube-confined reinforced UHPC columns under axial loading", *Eng. Struct.*, **230**, 111599. doi: 10.1016/j.engstruct.2020.111599.

Xu, W., Pan, G., Moradi, Z. and Shafiei, N. (2021), "Nonlinear forced vibration analysis of functionally graded non-uniform cylindrical microbeams applying the semi-analytical solution", *Compos. Struct.*, **275**, 114395. https://doi.org/10.1016/j.compstruct.2021.114395.

Xiao, X., Bu, G., Ou, Z. and Li, Z. (2022a), "Nonlinear in-plane instability of the confined FGP arches with nanocomposites reinforcement under radially-directed uniform pressure", *Eng. Struct.*, **252**, 113670. https://doi.org/10.1016/j.engstruct.2021.113670.

Xiao, G., Chen, B., Li, S. and Zhuo, X. (2022b), "Fatigue life analysis of aero-engine blades for abrasive belt grinding considering residual stress". *Eng. Fail. Analys.*, **131**, 105846. https://doi.org/10.1016/j.engfailanal.2021.105846.

Yu, X., Sun, Y., Zhao, D. and Wu, S. (2021), "A revised contact stiffness model of rough curved surfaces based on the length scale". *Tribology. Int.*, **164**. https://doi.org/10.1016/j.triboint.2021.107206.

Yang, M., Li, C., Zhang, Y., Jia, D., Zhang, X., Hou, Y., Li, R. and Wang, J. (2017), "Maximum undeformed equivalent chip thickness for ductile-brittle transition of zirconia ceramics under different lubrication conditions", *Int. J. Mach. Tool. Manufact.*, **122**, 55-65.

Yang, M., Li, C., Zhang, Y., Jia, D., Li, R., Hou, Y., Cao, H. and Wang, J. (2019a), "Predictive model for minimum chip thickness and size effect in single diamond grain grinding of zirconia ceramics under different lubricating conditions", *Ceram. Int.*, **45**(12), 14908-14920.

Yang, M., Li, C., Zhang, Y., Jia, D., Li, R., Hou, Y. and Cao, H. (2019b). "Effect of friction coefficient on chip thickness models in ductile-regime grinding of zirconia ceramics", *The. Int. J. Adv. Manufact. Techn.*, **102**(5), 2617-2632.

Zaitoun, M.W., Chikh, A., Tounsi, A., Al-Osta, M.A., Sharif, A., Al-Dulaijan, S.U. and Al-Zahrani, M.M. (2022), "Influence of the visco-Pasternak foundation parameters on the buckling behavior of a sandwich functional graded ceramic–metal plate in a hygrothermal environment", *Thin-Wall. Struct.*, **170**, 108549. https://doi.org/10.1016/j.tws.2021.108549.

Zaitoun, M.W., Chikh, A., Tounsi, A., Sharif, A., Al-Osta, M.A., Al-Dulaijan, S.U. and Al-Zahrani, M.M. (2021), "An efficient computational model for vibration behavior of a functionally graded sandwich plate in a hygrothermal environment with viscoelastic foundation effects", *Eng. Comput.*, 1-15. https://doi.org/10.1007/s00366-021-01498-1.

Zenkour, A.M. (2009), "The refined sinusoidal theory for FGM plates on elastic foundations", *Int. J. Mech. Sci.*, **51**(11-12), 869-880. https://doi.org/10.1016/j.ijmecsci.2009.09.026.

Zenkour, A.M. (2018), "Bending of thin rectangular plates with variable-thickness in a hygrothermal environment", *Thin-Wall. Struct.*, **123**, 333-340. https://doi.org/10.1016/j.tws.2017.11.038.

Zhang, L., Chen, Z., Habibi, M., Ghabussi, A. and Alyousef, R. (2021a), "Low-velocity impact, resonance, and frequency responses of FG-GPLRC viscoelastic doubly curved panel", *Compos. Struct.*, **269**, 114000. https://doi.org/10.1016/j.compstruct.2021.114000.

Zhang, W. and Tang, Z. (2021b). "Numerical modeling of response of CFRP–concrete interfaces subjected to fatigue loading", *J. Compos. Construct.*, **25**(5). https://doi.org/10.1061/(ASCE)CC.1943-5614.0001154.

Zhang, H., Liu, Y. and Deng, Y. (2021c), "Temperature gradient modeling of a steel box-girder suspension bridge using Copulas probabilistic method and field monitoring", *Adv. Struct. Eng.*, **24**(5), 947-961. https://doi.org/10.1177/1369433220971779.

Zhang, Y., Li, C., Ji, H., Yang, X., Yang, M., Jia, D., Zhang, X., Li, R. and Wang, J. (2017), "Analysis of grinding mechanics and improved predictive force model based on material-removal and plastic-stacking mechanisms", *Int. J. Mach. Tool. Manufact.*, **122**, 81-97.

Zhang, D., Li, C., Zhang, Y., Jia, D. and Zhang, X. (2015), "Experimental research on the energy ratio coefficient and specific grinding energy in nanoparticle jet MQL grinding", *The. Int. J. Adv. Manufact. Techn.*, **78**(5), 1275-1288.

Zhang, J., Li, C., Zhang, Y., Yang, M., Jia, D., Liu, G., Hou, Y., Li, R., Zhang, N., Wu, Q. and Cao, H. (2018), "Experimental assessment of an environmentally friendly grinding process using nanofluid minimum quantity lubrication with cryogenic air", *J. Cleaner. Product.*, **193**, 236-248.

Zhang, S., Pak, R.Y.S. and Zhang, J. (2021), "Three-dimensional frequency-domain Green's functions of a finite fluid-saturated soil layer underlain by rigid bedrock to interior loadings". *Int. J. Geomech.*, **22**(1), https://doi.org/10.1061/(ASCE)GM.1943-5622.0002235.

Zhang, S.W., Shang, L.Y., Zhou, L. and Lv, Z.B. (2022), "Hydrate deposition model and flow assurance technology in gas-dominant pipeline transportation systems: A review", *Energ. Fuel.*, https://doi.org/10.1021/acs.energyfuels.1c03812

Zhao, Y., Moradi, Z., Davoudi, M. and Zhuang, J. (2021a), "Bending and stress responses of the hybrid axisymmetric system via state-space method and 3D-elasticity theory", *Eng. Comput.*, 1-23. https://doi.org/10.1007/s00366-020-01242-1.

Zhao, T.H. Khan, M.I. and Chu, Y.M. (2021b), "Artificial neural networking (ANN) analysis for heat and entropy generation in flow of non-Newtonian fluid between two rotating disks", *Math. Meth. Appl. Sci.*, https://doi.org/10.1002/mma.7310

Zhao, T.H., Khan, M.I. and Chu, Y.M. (2021c), "Artificial neural networking (ANN) analysis for heat and entropy generation in flow of non-Newtonian fluid between two rotating disks", *Math. Meth. Appl. Sci.*, https://doi.org/10.1002/mma.7310.

Zhong, Z. and Shang, E. (2008), "Closed-form solutions of three-dimensional functionally graded plates", *Mech. Adv. Mater. Struct.*, **15**(5), 355-363. https://doi.org/10.1080/15376490801977528.

CC

Appendix A

$$\alpha_1=\int_{-\frac{h(x)}{2}}^{\frac{h(x)}{2}}\frac{E(z)}{2(1+\nu)}dz,\quad \alpha_2=\int_{-\frac{h(x)}{2}}^{\frac{h(x)}{2}}\frac{E(z)z^2}{2(1+\nu)}dz,$$

$$\alpha_3=\int_{-\frac{h(x)}{2}}^{\frac{h(x)}{2}}\frac{E(z)z^4}{2(1+\nu)}dz,\alpha_4=\int_{-\frac{h(x)}{2}}^{\frac{h(x)}{2}}\frac{E(z)z^4}{1-\nu^2}dz$$

$$\alpha_5=\int_{-\frac{h(x)}{2}}^{\frac{h(x)}{2}}\frac{E(z)z^6}{1-\nu^2}dz,\alpha_{13}=\int_{-\frac{h(x)}{2}}^{\frac{h(x)}{2}}\frac{E(z)z^6}{2(1+\nu)}dz,\alpha_6=\alpha_4-c\alpha_5$$

$$\alpha_{12}=\int_{-\frac{h(x)}{2}}^{\frac{h(x)}{2}}\frac{E(z)z^2}{1-\nu^2}dz,$$

$$\alpha_7=-c\alpha_5,\quad \alpha_8=-c_x\alpha_5,\quad \alpha_9=\alpha_3-c\alpha_{13},\quad \alpha_{10}=-2c\alpha_{13},$$

$$\alpha_{11}=-c_x\alpha_{13}$$

$$Z_1=\alpha_{1x}-3c_x\alpha_2-3c\alpha_{2x}-3c\left(\alpha_{2x}-3c_x\alpha_3-3c\alpha_{3x}\right)+c\alpha_{8xx}$$

$$Z_2=\alpha_1-3c\alpha_2-3c\left(\alpha_2-3c\alpha_3\right)+c\left(2\alpha_{8x}+\alpha_{6xx}\right)$$

$$Z_3=c\left(2\alpha_{6x}+\alpha_8\right),\quad Z_4=c\alpha_6,\quad Z_5=2c\alpha_9+\nu c\alpha_6,$$

$$Z_6=2c\alpha_{9x}+\nu c\alpha_8$$

$$Z_7=\alpha_1-3c\alpha_2-3c\left(\alpha_2-3c\alpha_3\right)+\nu c\alpha_{6xx}+2c\alpha_{11x},$$

$$Z_8=2\nu c\alpha_{6x}+2c\alpha_{9x}+2c\alpha_{11}$$

$$Z_9=\nu c\alpha_6+2c\alpha_9,\quad Z_{10}=c\alpha_6,\quad Z_{11}=\alpha_{1x}-3c_x\alpha_2-3c\alpha_{2x}$$

$$-3c\left(\alpha_{2x}-3c_x\alpha_3-3c\alpha_{3x}\right)$$

$$Z_{12}=\alpha_1-3c\alpha_2-3c\left(\alpha_2-3c\alpha_3\right)+c\left(\alpha_{7xx}+2\alpha_{8x}\right),$$

$$Z_{13}=c\left(2\alpha_{7x}+\alpha_8\right),Z_{14}=c\alpha_7$$

$$Z_{15}=2\nu c\alpha_{7x}+2c\alpha_{10x}+2c\alpha_{11}+\nu c\alpha_8,\quad Z_{16}=2\nu c\alpha_7+2c\alpha_{10},$$

$$Z_{17}=c\alpha_7$$

$$Z_{18}=\alpha_1-3c\alpha_2-3c\left(\alpha_2-3c\alpha_3\right)+\nu c\alpha_{7xx}+2c\alpha_{11x}$$

$$R_1=\alpha_{2x}-c_x\alpha_3-c\alpha_{3x}-\nu c_x\alpha_4-c\alpha_{9x},$$

$$R_2=\alpha_2-c\alpha_3+\nu\left(\alpha_{12}-c\alpha_4\right)-c\alpha_9-\nu c\alpha_6$$

$$R_1=\alpha_{2x}-c_x\alpha_3-c\alpha_{3x}-\nu c_x\alpha_4-c\alpha_{9x},$$

$$R_2=\alpha_2-c\alpha_3+\nu\left(\alpha_{12}-c\alpha_4\right)-c\alpha_9-\nu c\alpha_6$$

$$R_3=-c_{xx}\alpha_3-c_x\alpha_{3x}-c\alpha_{11x}-(\alpha_1-3c\alpha_2)+3c(\alpha_2-3c\alpha_3),$$

$$R_4=\alpha_{2x}-2c_x\alpha_3-c\alpha_{3x}-c\alpha_{9x}-c\alpha_{11}$$

$$R_5=\alpha_2-\left(\alpha_3+\alpha_9\right),\quad R_6=\alpha_{12}-2(\alpha_4+\alpha_6)$$

$$R_7=-c_{xx}\alpha_3-c_x\alpha_{3x}-c\alpha_{11x}-\left(\alpha_1-3c\alpha_2\right)+3c\left(\alpha_2-3c\alpha_3\right)$$

$$R_8=-2(c_x\alpha_3+c\alpha_{3x})-c_x\alpha_3-\nu c_x\alpha_4-c\alpha_{10x}-c\alpha_{11}-\nu c\alpha_8,$$

$$R_9=-2c\alpha_3-\nu c\alpha_4-c\alpha_{10}-\nu c\alpha_7$$

$$R_{10}=-c\left(\alpha_4+\alpha_7\right)$$

$$S_1=-\left(c_{xx}\alpha_4+c_x\alpha_{4x}\right)-c\alpha_{8x}-\left(\alpha_1-3c\alpha_2\right)+3c\left(\alpha_2-3c\alpha_3\right)$$

$$S_2=\alpha_{12x}-2c_x\alpha_4-c\alpha_{4x}-c\alpha_{6x}-c\alpha_8,\quad S_3=\alpha_{12}-c\left(\alpha_4+\alpha_6\right)$$

$$S_4=\alpha_2-c\left(\alpha_3+\alpha_9\right),\quad S_5=\nu\left(\alpha_{12x}-c_x\alpha_4-c\alpha_{4x}\right)-c_x\alpha_3-\nu c\alpha_{6x}-c\alpha_{11}$$

$$S_6=\nu\left(\alpha_{12}-c\alpha_4\right)-\nu c\alpha_6+\alpha_2-c\left(\alpha_3+\alpha_9\right),$$

$$S_7=-\left(c_{xx}\alpha_4+c_x\alpha_{4x}\right)-c\alpha_{8x}\left(\alpha_1-3c\alpha_2\right)+3c\left(\alpha_2-3c\alpha_3\right)$$

$$S_8=-\left(2c_x\alpha_4+c\alpha_{4x}\right)-c\alpha_{7x}-c\alpha_8,\quad S_9=-c\left(\alpha_4+\alpha_7\right)$$

$$S_{10}=-\nu c\left(\alpha_4+\alpha_7\right)-2c\alpha_3-c\alpha_{10},\quad S_{11}=-\nu\left(c_x\alpha_4+c\alpha_{4x}\right)-c_x\alpha_3-\nu c\alpha_{7x}-c\alpha_{11}$$

$$M^T=\int_{-\frac{h(x)}{2}}^{\frac{h(x)}{2}}E(z)\alpha(z)\Delta T(z)zdz,$$

$$M^{3T}=\int_{-\frac{h(x)}{2}}^{\frac{h(x)}{2}}E(z)\alpha(z)\Delta T(z)z^3dz$$

$$Q_x=\left(\alpha_1-3c\alpha_2\right)\left(\varphi+w_x\right),\quad Q_y=\left(\alpha_1-3c\alpha_2\right)\left(\psi+w_y\right)$$

$$R_x=\left(\alpha_2-3c\alpha_3\right)\left(\varphi+w_x\right),\quad R_y=\left(\alpha_2-3c\alpha_3\right)\left(\psi+w_y\right)$$

$$P_x=\alpha_6\left(\varphi_x+\nu\psi_y\right)+\alpha_7\left(w_{xx}+\nu w_{yy}\right)+\alpha_8\left(\varphi+w_x\right)-\frac{M^{3T}}{1-\nu}$$

$$P_y=\alpha_6\left(\psi_y+\nu\varphi_x\right)+\alpha_7\left(w_{yy}+\nu w_{xx}\right)+\nu\alpha_8\left(\varphi+w_x\right)-\frac{M^{3T}}{1-\nu}$$

$$P_{xy}=\alpha_9\left(\varphi_y+\psi_x\right)+\alpha_{10}w_{xy}+\alpha_{11}\left(\psi+w_y\right)$$

$$M_x=\left(\alpha_{12}-c\alpha_4\right)\left(\varphi_x+\nu\psi_y\right)-c\alpha_4\left(w_{xx}+\nu w_{yy}\right)$$

$$-c_x\alpha_4\left(\varphi+w_x\right)-\frac{M^T}{1-\nu}$$

$$M_y=(\alpha_{12}-c\alpha_4)(\psi_y+\nu\varphi_x)-c\alpha_4(w_{yy}+\nu w_{xx})-\nu c_x\alpha_4(\varphi+w_x)-\frac{M^T}{1-\nu}$$

$$M_{xy}=(\alpha_2-c\alpha_3)(\varphi_y+\psi_x)-2c\alpha_3w_{xy}-c_x\alpha_3(\psi+w_y)$$